

Prediction of several Co-based $\text{La}_3\text{Ni}_2\text{O}_7$ -like superconducting materials

Jing-Xuan Wang,^{1,2,*} Yi-Heng Tian,^{1,2,*} Jian-Hong She,^{1,2,*} Rong-Qiang He,^{1,2,†} and Zhong-Yi Lu^{1,2,3,‡}

¹*School of Physics and Beijing Key Laboratory of Opto-electronic Functional Materials & Micro-nano Devices, Renmin University of China, Beijing 100872, China*

²*Key Laboratory of Quantum State Construction and Manipulation (Ministry of Education), Renmin University of China, Beijing 100872, China*

³*Hefei National Laboratory, Hefei 230088, China*

(Dated: September 12, 2025)

High temperature superconductivity has been found in Fe, Ni, and Cu compounds, but not Co, where the Ni compounds include the recently found bilayer nickelate $\text{La}_3\text{Ni}_2\text{O}_7$ under high pressure. Here we theoretically predict several Co-based $\text{La}_3\text{Ni}_2\text{O}_7$ -like high-temperature superconducting materials. With electron doping to high-pressure bilayer cobaltate $\text{La}_3\text{Co}_2\text{O}_7$, we find that $\text{LaTh}_2\text{Co}_2\text{O}_7$, $\text{La}_3\text{Ni}_2\text{O}_5\text{Cl}_2$, and $\text{La}_3\text{Ni}_2\text{O}_5\text{Br}_2$ may show similar crystal structures and strongly correlated electronic structures to bilayer nickelate $\text{La}_3\text{Ni}_2\text{O}_7$ under high pressure. Within the random-phase approximation (RPA), the leading pairing symmetry in these materials is *s*-wave.

Introduction. Since the discovery of cuprate superconductors, their unconventional superconducting properties have attracted enormous interest [1–4]. Subsequent discoveries of high temperature superconducting phases in Fe-based and Ni-based compounds have highlighted the role of strong correlations in 3d transition-metal systems [5–11]. The nickelates were theoretically predicted to exhibit superconductivity by analogy with cuprates, and some materials have also been experimentally confirmed in recent years [12–15]. The successful extension of superconductivity from cuprates to nickelates provides a promising direction for the exploration of other transition metal-based superconductors. Recently, nickelates $\text{La}_3\text{Ni}_2\text{O}_7$ have emerged as promising analogs, exhibiting correlation-driven instabilities that may underpin superconductivity [10]. However, investigating isoelectronic systems beyond nickel—such as cobaltates, where Co exhibits tunable spin states—could reveal novel routes to high- T_c superconductivity.

The discovery of cobaltate superconductivity dates back to 2003, when superconductivity with a transition temperature of 3 K was first reported in the layered cobaltate $\text{Na}_x\text{CoO}_2\cdot\text{H}_2\text{O}$ [16]. Its superconducting pairing symmetry has not yet been confirmed and tends to be an unconventional superconductor [17]. However, the precise control required for the Na concentration and water content in this material makes it challenging to achieve a single-phase sample [18]. More recently, by substituting CoO_2 with CoSe_2 as the conducting layer, researchers successfully synthesized $\text{Na}_2\text{CoSe}_2\text{O}$, which exhibits a superconducting transition temperature of 6.3 K [19]. Although the material shows unusual physical properties, such as quasi-two-dimensionality, low carrier concentration, and an exceptionally high upper critical field, recent research has suggested that it likely exhibits conventional superconductivity [20]. Despite these advances, high-temperature unconventional superconductivity has not yet been established in cobaltates, leaving a conspicuous absence relative to other 3d transition-metal

oxides. Strong-correlation theory is crucial for elucidating the superconducting mechanism in nickelates and for probing other unconventional superconductors with similar electronic structures.

In this Letter, we theoretically predict cobaltate bilayer compounds as promising high-temperature superconductor candidates by electron doping the high-pressure phase of $\text{La}_3\text{Co}_2\text{O}_7$. By analogy with $\text{La}_3\text{Ni}_2\text{O}_7$, we used density functional theory plus dynamical mean-field theory (DFT+DMFT) and random-phase approximation (RPA) methods [21, 22] to calculate and study the electronic structure, electronic correlation, and superconductivity of $\text{LaTh}_2\text{Co}_2\text{O}_7$ and $\text{La}_3\text{Co}_2\text{O}_5\text{Cl}_2$. For these materials, their band structures are very similar to that of $\text{La}_3\text{Ni}_2\text{O}_7$, and their orbitals exhibit correlations and occupation numbers comparable to those in $\text{La}_3\text{Ni}_2\text{O}_7$. The results reveal that Th- and Cl-doped $\text{La}_3\text{Co}_2\text{O}_7$ exhibit strongly correlated electronic structures, characterized by Hund correlation and large mass enhancement, which promotes the emergence of superconductivity. Our findings suggest that pressure and doping can potentially induce high-temperature superconductivity in these cobaltates, paralleling the nickelates.

Similar crystal structures. To enable a direct comparison with the $\text{La}_3\text{Ni}_2\text{O}_7$ superconductor under a high pressure of 29.5 GPa, we optimized $\text{La}_3\text{Co}_2\text{O}_7$ under 25 GPa and obtained comparable lattice constants, as shown in Table S1 of the Supplemental Material (SM) [23]. The space group of $\text{La}_3\text{Co}_2\text{O}_7$ belongs $I4/mmm$, with lattice parameters $a = 3.703 \text{ \AA}$ and $c = 19.174 \text{ \AA}$ under 25 GPa. In addition, both the bond lengths and the bond angles between the transition-metal and O atoms in the two materials are comparable. To confirm the dynamical stability, we calculated the phonon spectra using DFT, finding no imaginary phonon modes and thus indicating robust structural stability (see Fig. S2 in the SM).

However, the Co atom in $\text{La}_3\text{Co}_2\text{O}_7$ has a valence of +2.5 with a $3d^{6.5}$ electronic configuration, whereas the Ni atom in $\text{La}_3\text{Ni}_2\text{O}_7$ has a $3d^{7.5}$ configuration. To

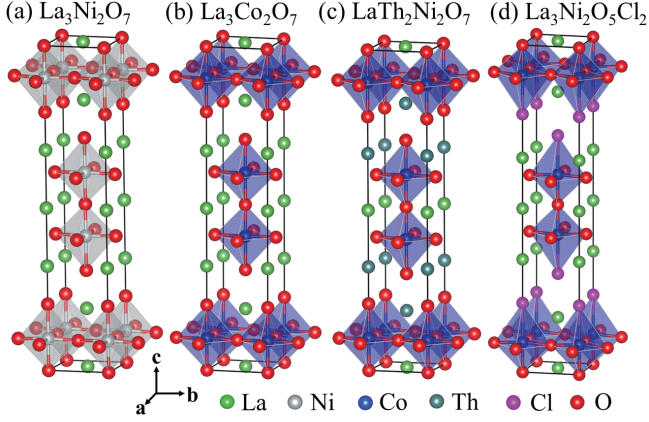


Figure 1. Crystal structure of (a) $\text{La}_3\text{Ni}_2\text{O}_7$, (b) $\text{La}_3\text{Co}_2\text{O}_7$, (c) $\text{LaTh}_2\text{Co}_2\text{O}_7$, and (d) $\text{La}_3\text{Co}_2\text{O}_5\text{Cl}_2$ at high pressure.

achieve a comparable $3d^{7.5}$ configuration for Co, we substituted +4-valent Th atom at the La site and -1-valent Cl atom at the O site, effectively reducing the Co valance from +2.5 to +1.5. In $\text{LaTh}_2\text{Co}_2\text{O}_7$, the in-plane Co-O bond lengths within the CoO_6 octahedra match those in $\text{La}_3\text{Ni}_2\text{O}_7$, while the apical Co-O bond lengths are elongated by approximately 2% relative to those in $\text{La}_3\text{Ni}_2\text{O}_7$. By contrast, in $\text{La}_3\text{Co}_2\text{O}_5\text{Cl}_2$, the in-plane bond lengths are similar to those in the Th-doped compound, but one of the axial Co-O bond lengths is significantly longer (by about 25%) than that in $\text{La}_3\text{Ni}_2\text{O}_7$, attributable to the less charge of the Cl anion relative to O anion. See more details in the SM.

Similar electronic structures. The key to predicting superconducting materials lies in identifying favorable electronic structures. Fig. 2 presents band structures of $\text{La}_3\text{Ni}_2\text{O}_7$, $\text{LaTh}_2\text{Co}_2\text{O}_7$ and $\text{La}_3\text{Co}_2\text{O}_5\text{Cl}_2$ obtained by DFT and DFT+DMFT calculations. Among the three materials, the energy bands of the Ni/Co e_g orbitals are similar, and the e_g -orbital bands have a bandwidth of approximately 3.8 eV, spanning from -1.2 to 2.6 eV for Ni and from -0.8 to 3.0 eV for Co. Unlike in the nickelate, the bands near the Fermi level in Th- and Cl-doped cobaltates are less pure, with contributions from other orbitals. In $\text{La}_3\text{Ni}_2\text{O}_7$, the La $5d$ bands extend down to about 0.9 eV above the Fermi level, whereas the Th $4f$ bands in $\text{LaTh}_2\text{Co}_2\text{O}_7$ cross the Fermi level down to about -1.4 eV, forming a pocket at the Γ point dominated by Th orbitals. Similarly, the La $5d$ bands in $\text{La}_3\text{Co}_2\text{O}_5\text{Cl}_2$ appear near the Fermi level. The electron occupation in these La $5d$ or Th $4f$ bands, analogous to the self-doping effect in LaNiO_2 , may not impact their potential superconductivity. In the lower panels, the momentum-resolved spectral functions calculated by DFT+DMFT at 290 K show that the correlated-orbital bands become blurred. The strong renormalization due to correlations narrows the bandwidth for both $\text{LaTh}_2\text{Co}_2\text{O}_7$ and $\text{La}_3\text{Co}_2\text{O}_5\text{Cl}_2$, resulting in a flat band at the Fermi level. These results

consistent with those for $\text{La}_3\text{Ni}_2\text{O}_7$.

The upper panel of Fig. 3 shows the Fermi surface of $\text{La}_3\text{Ni}_2\text{O}_7$, $\text{LaTh}_2\text{Co}_2\text{O}_7$, and $\text{La}_3\text{Co}_2\text{O}_5\text{Cl}_2$ obtained from DFT+DMFT calculations at 290 K. For $\text{La}_3\text{Ni}_2\text{O}_7$, the Fermi surface features an electron-like α pocket around the center of the Brillouin zone (Γ), a hole-like β pocket around the zone corner (M), and a prominent hole-like γ pocket near the M point. Unlike in the nickelate, the Fermi surface of $\text{LaTh}_2\text{Co}_2\text{O}_7$ exhibits electronic states at the Γ point and appears as a broken arc, reflecting the destruction of the Fermi-liquid coherence induced by doping. For $\text{La}_3\text{Co}_2\text{O}_5\text{Cl}_2$, the Fermi surface consists of two electron-like pockets around the Γ point and a hole-like pocket around the M point.

Similarly strong correlation. To insight correlation effect, Fig. 4 presents the imaginary part of self-energy, $\text{Im}\Sigma(i\omega_n)$, at Matsubara frequencies for the Co e_g orbitals in Th- and Cl-doped $\text{La}_3\text{Co}_2\text{O}_7$, compared with that for the Ni e_g orbitals in $\text{La}_3\text{Ni}_2\text{O}_7$. For both Th- and Cl-doped $\text{La}_3\text{Co}_2\text{O}_7$, the $\text{Im}\Sigma(i\omega_n)$ values of the Co d_{z^2} orbitals are similar across frequencies, as are those of the $d_{x^2-y^2}$ orbitals. This indicates that both doping strategies effectively enable electronic control within the Co e_g manifold.

In both Th- and Cl-doped cobaltates, the self-energies of the d_{z^2} and $d_{x^2-y^2}$ orbitals exhibit a linear frequency dependence with a finite intercept at low frequencies, signaling non-Fermi-liquid behavior. In addition, the magnitudes of $\text{Im}\Sigma(i\omega_n)$ for the d_{z^2} orbitals are larger than those of the $d_{x^2-y^2}$ orbitals, suggesting stronger correlations in the former. These features align with the behavior observed for Ni in $\text{La}_3\text{Ni}_2\text{O}_7$.

The obvious difference is that the magnitudes of $\text{Im}\Sigma(i\omega_n)$ for the d_{z^2} and $d_{x^2-y^2}$ orbitals of Ni in $\text{La}_3\text{Ni}_2\text{O}_7$ are more comparable, whereas a clearly separation is observed for the corresponding Co orbitals in Th- and Cl-doped cobaltates. This disparity arises from local structural distortions induced by Th or Cl doping. Specifically, doping leads to axial elongation of the CoO_6 octahedra, increasing the ratio of apical to in-plane Co-O bond lengths compared to the NiO_6 octahedra in $\text{La}_3\text{Ni}_2\text{O}_7$ (see Table S1). This elongation enhances the crystal-field splitting within the e_g manifold, lowering the energy of the d_{z^2} orbital relative to $d_{x^2-y^2}$, thereby amplifying the low-frequency self-energy differences between these two orbitals.

Table II lists the occupation numbers N_d and effective mass enhancements $1/Z$ of e_g orbitals for $\text{La}_3\text{Ni}_2\text{O}_7$ and electron-doped $\text{La}_3\text{Co}_2\text{O}_7$. In $\text{La}_3\text{Ni}_2\text{O}_7$, the N_d and $1/Z$ values for the e_g orbital are consistent with previous results [25]. For both Ni in $\text{La}_3\text{Ni}_2\text{O}_7$ and Co in the doped cobaltates, the occupation numbers of the e_g orbital are exceed the nominal value of 1.5, which is caused by hybridization between Ni or Co atoms and O atoms. Furthermore, the occupancy numbers of the e_g orbital for Co atom in Th-, Cl-, Br-doped $\text{La}_3\text{Co}_2\text{O}_7$ are approx-

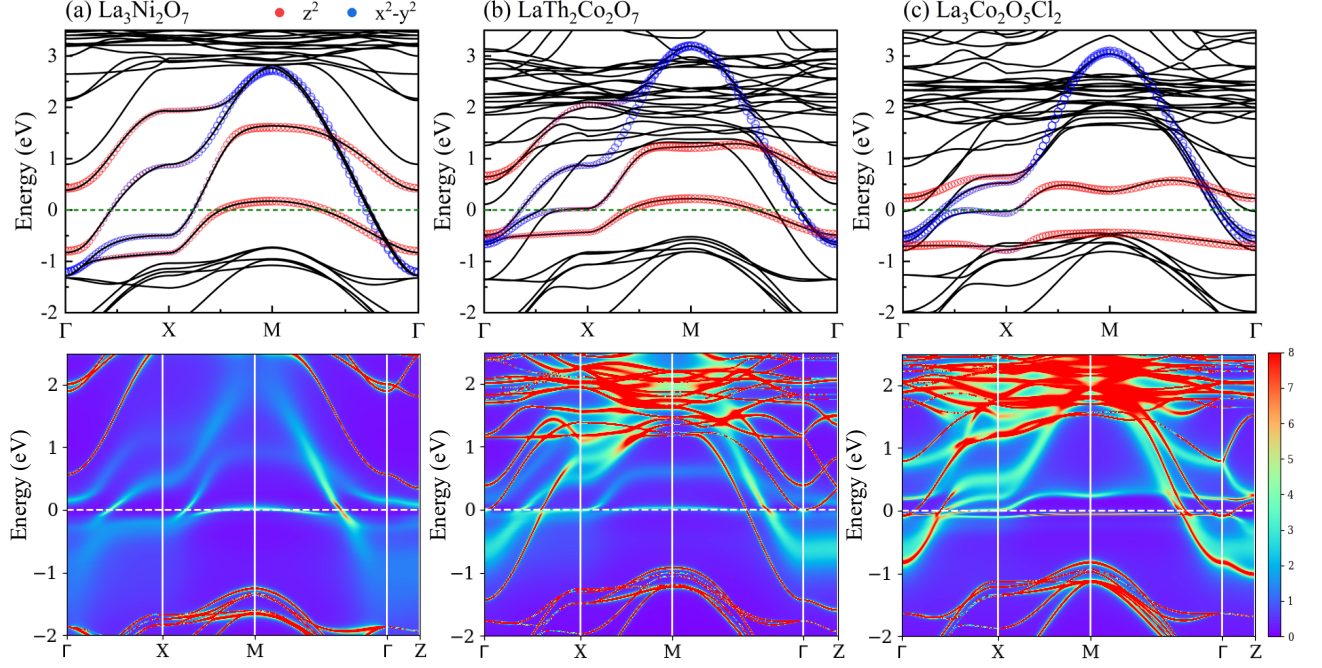


Figure 2. Band structures of $\text{La}_3\text{Ni}_2\text{O}_7$, $\text{LaTh}_2\text{Co}_2\text{O}_7$, and $\text{La}_3\text{Co}_2\text{O}_5\text{Cl}_2$. The orbital-resolved bands calculated by DFT are shown in the upper panels. The band structure of the bilayer two-orbital tight-binding models is superposed, where the orbital weights are represented by the size of the colored circles. The momentum-resolved spectral functions $A(\mathbf{k}, \omega)$ obtained by DFT+DMFT at 290 K are displayed in the lower panels. The dashed green and blue lines at 0 eV denote the Fermi level.

Table I. Main parameters of our bilayer two-orbital TB models, compared with Ref. [24]. The remaining parameters for longer hoppings are provided in the SM.

	t_1^x	t_1^z	t_2^x	t_2^z	t_3^{xz}	t_\perp^x	t_\perp^z	t_4^{xz}	ϵ^x	ϵ^z
$\text{La}_3\text{Ni}_2\text{O}_7$ [24]	-0.483	-0.110	0.069	-0.017	0.239	0.005	-0.635	-0.034	0.776	0.409
$\text{La}_3\text{Ni}_2\text{O}_7$	-0.492	-0.135	0.059	-0.011	0.253	-0.013	-0.670	-0.043	0.721	0.470
$\text{LaTh}_2\text{Co}_2\text{O}_7$	-0.478	-0.078	0.057	-0.001	0.196	-0.090	-0.578	-0.058	1.168	0.494
$\text{La}_3\text{Co}_2\text{O}_5\text{Cl}_2$	-0.459	-0.026	0.112	0.005	0.087	0.017	-0.495	0.004	1.000	-0.070

Table II. Local orbital occupation number N_d and effective mass enhancement $1/Z$ of the Ni and Co atoms in $\text{La}_3\text{Ni}_2\text{O}_7$, $\text{LaTh}_2\text{Co}_2\text{O}_7$, and $\text{La}_3\text{Co}_2\text{O}_5\text{Cl}_2$ at high pressure for the d_{z^2} and $d_{x^2-y^2}$ orbitals at 290 K.

	N_d		$1/Z$	
	d_{z^2}	$d_{x^2-y^2}$	d_{z^2}	$d_{x^2-y^2}$
Ni in $\text{La}_3\text{Ni}_2\text{O}_7$	1.136	1.056	2.52	2.02
Co in $\text{LaTh}_2\text{Co}_2\text{O}_7$	0.938	0.748	5.81	4.02
Co in $\text{La}_3\text{Co}_2\text{O}_5\text{Cl}_2$	1.004	0.726	3.33	2.93
Co in $\text{La}_3\text{Co}_2\text{O}_5\text{Br}_2$	1.001	0.719	2.13	2.89

imately 1.7, lower than that in $\text{La}_3\text{Ni}_2\text{O}_7$, likely due to elongated Co-O bonds upon doping, which reduce charge transfer from O to Co. Among these materials, the ef-

Table III. The weights (%) of the Ni- and Co- e_g orbital local multiplets for $\text{La}_3\text{Ni}_2\text{O}_7$ and $\text{La}_3\text{Co}_2\text{O}_7$ with Th, Cl and Br-doped respectively calculated by DFT+DMFT at 290 K. The good quantum numbers N_Γ and S_z denote the total occupancy and total spin of the Ni- and Co- e_g orbital, which are used to label different local spin states.

N_Γ	0	1	2	2	3	4	
S_z	0	1/2	0	1	1/2	0	$\sqrt{\langle S_z^2 \rangle}$
Ni in $\text{La}_3\text{Ni}_2\text{O}_7$	0.0	12.4	23.6	33.3	28.1	2.3	0.658
Co in $\text{LaTh}_2\text{Co}_2\text{O}_7$	2.5	36.2	21.4	30.3	9.2	0.3	0.645
Co in $\text{La}_3\text{Co}_2\text{O}_5\text{Cl}_2$	2.2	33.6	22.7	30.9	10.2	0.4	0.647
Co in $\text{La}_3\text{Co}_2\text{O}_5\text{Br}_2$	2.4	34.1	23.4	29.5	10.2	0.4	0.637

fective mass enhancement of the d_{z^2} and $d_{x^2-y^2}$ orbitals

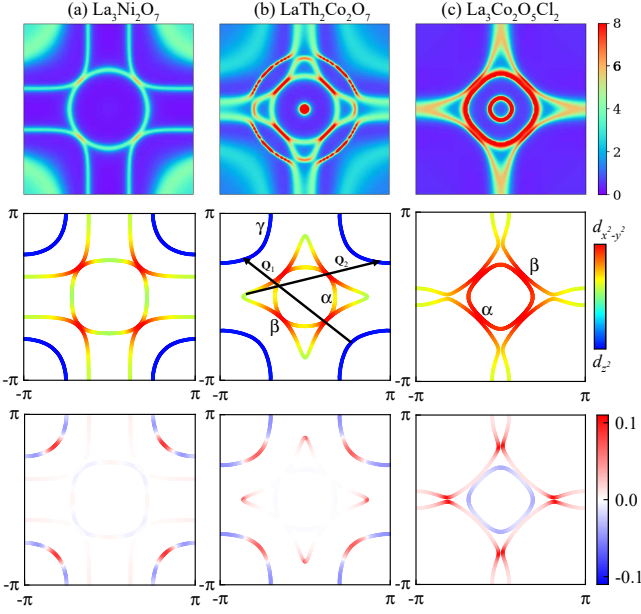


Figure 3. The upper panels show the Fermi surfaces for (a) $\text{La}_3\text{Ni}_2\text{O}_7$, (b) $\text{LaTh}_2\text{Co}_2\text{O}_7$, and (c) $\text{La}_3\text{Co}_2\text{O}_5\text{Cl}_2$ calculated by DFT+DMFT. The middle panels show the orbital-resolved Fermi surfaces of the corresponding TB models. The lower panels show the superconducting gap structures on the Fermi surfaces calculated with RPA on the three TB models with $U = 1.4, 0.9$, and 1 eV, respectively.

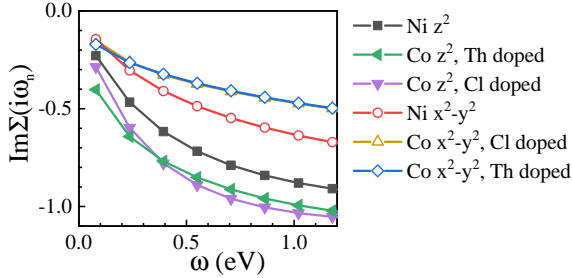


Figure 4. (a) The imaginary parts at the Matsubara axis $\text{Im}\Sigma(i\omega_n)$ of the self-energy functions for (a) $\text{La}_3\text{Ni}_2\text{O}_7$, (b) $\text{La}_3\text{Co}_2\text{O}_7$, (c) $\text{LaTh}_2\text{Co}_2\text{O}_7$, and (d) $\text{La}_3\text{Co}_2\text{O}_5\text{Cl}_2$ at 290 K.

exceed 2, indicating strong orbital-selective correlations. In $\text{LaTh}_2\text{Co}_2\text{O}_7$, the effective mass enhancement for both d_{z^2} and $d_{x^2-y^2}$ is markedly higher than in other compounds, suggesting proximity to quantum-critical behavior under this doping. For the Th- and Cl-doped cobaltates, further pressure tuning could modulate their effective masses, potentially suppressing electron localization.

For Th- and Cl-doped $\text{La}_3\text{Co}_2\text{O}_7$, both the low-spin state ($N_\Gamma=1$, $S_z=1/2$) and the high-spin state ($N_\Gamma=2$, $S_z=1$) exhibit substantial weights (shown in Table III), signaling a doping-induced transition of Co from a predominantly low-spin configuration to a mixed high-spin/low-spin state. This dispersed weight distribution points to enhanced spin fluctuations which is essential for

high T_c superconductivity. Moreover, recent theoretical work on the phase diagram of nickelate superconductors [26] has established the local spin moment, $\langle S_z^2 \rangle$, as a crucial descriptor for the strength of these fluctuations. Their findings indicate that these high- T_c superconductors emerge within a narrow window of $\langle S_z^2 \rangle$ values (approximately 0.63 to 0.68). Systems with moments that are too high enter a spin-density-wave (SDW) state, while those with moments that are too low behave as Fermi liquids. Our designed cobaltate systems are analogous to $\text{La}_3\text{Ni}_2\text{O}_7$, relying on a similar principle of Hund's coupling-enhanced, two-orbital strong correlations. Remarkably, our calculated $\langle S_z^2 \rangle$ values, ranging from 0.637 to 0.647, fall precisely within this optimal superconducting window. This alignment provides strong theoretical support for the possibility of realizing high-temperature superconductivity in these cobalt-based compounds.

Tight-binding models and their s-wave superconducting pairing symmetry. We construct the tight-binding (TB) models by fitting to the e_g bands from our DFT calculations via a least-squares method. The details of the fitting are presented in the SM. The onsite energies $\epsilon_{x/z}$ and the hopping parameters are listed in Table I for $\text{LaTh}_2\text{Co}_2\text{O}_7$ and $\text{La}_3\text{Co}_2\text{O}_5\text{Cl}_2$, with $\text{La}_3\text{Ni}_2\text{O}_7$ included for comparison. As shown in Fig. 2, the TB models have captured the main characteristics of the Co- e_g orbitals near the Fermi level.

The central middle panel of Fig. 3 shows the Fermi surface of the TB model for $\text{LaTh}_2\text{Co}_2\text{O}_7$, which comprises three sheets (α , β , and γ). The static spin susceptibility (shown in the SM) exhibits prominent peaks at two inequivalent wavevectors Q_1 and Q_2 . Q_1 corresponds to the nesting between the γ pocket and itself, while Q_2 corresponds to the nesting between the β and γ pockets. The critical interaction strength U_c at which the spin susceptibility diverges is 1.01 eV, indicating the onset of SDW order. The leading superconducting gap function for $U = 0.9$ eV corresponds to the A_{1g} irreducible representation, which is hence of s wave, as shown in the middle right panel of Fig. 3.

The Fermi surface of the TB model for $\text{La}_3\text{Co}_2\text{O}_5\text{Cl}_2$ is shown in the lower central panel of Fig. 3. There are only two sheets, denoted as α and β . The dominant peak of the spin susceptibility corresponds to the wavevector that connects the α and β pockets. The critical interaction U_c for the divergence of the spin susceptibility is 1.07 eV. For an interaction strength of $U = 1$ eV, the leading pairing symmetry is found to be s_{\pm} -wave, and its corresponding gap function is shown in the lower right panel of Fig. 3.

Discussion. The discovery of nickel-based superconductivity has provided a new platform for the study of high-temperature superconductivity. Its distinct bilayer structure and superconducting mechanism, different from those of cuprates and iron-based superconductors, have broadened the diversity of high-temperature superconductivity. However, the absence of cobalt-based high-

temperature superconductivity has long been a challenge for the research community. In this work, we have predicted a new class of Co-based high-temperature superconductors that possess a crystal structure and strongly correlated electronic structure similar to $\text{La}_3\text{Ni}_2\text{O}_7$. It is anticipated that these materials will be synthesized experimentally in the near future, turning cobalt-based high-temperature superconductivity into a reality.

We constructed a bilayer two-orbital theoretical model for these Co-based materials. RPA calculations predict an s-wave pairing symmetry. In the future, other theoretical methods can be employed to conduct more detailed investigations of these models.

Given that bulk bilayer nickelate superconductors are often difficult to achieve superconductivity under ambient pressure and exhibit lower crystal symmetry and complex density wave orders, we expect that the cobalt-based materials may behave similarly under ambient pressure, which will be left for future studies.

Following the direction of our work, there are more potential Co-based superconducting materials worth exploring. One could consider replacing La in $\text{LaTh}_2\text{Co}_2\text{O}_7$ with other trivalent rare-earth elements, for which there are numerous candidates. Other methods of electron doping could be considered, such as hydrogen doping. For instance, Ref. [27] reported hydrogen doping in La_2NiO_4 with the aim of achieving electron-doped, single-orbital superconductivity in a nickel-based material. Both cuprate and iron-based superconductors comprise a large family of materials, and it is possible that cobalt-based superconductors will do as well. Furthermore, since $\text{La}_4\text{Ni}_3\text{O}_{10}$ also exhibits high-temperature superconductivity, one could attempt to design Co-based superconducting materials analogous to $\text{La}_4\text{Ni}_3\text{O}_{10}$. In $\text{La}_4\text{Ni}_3\text{O}_{10}$, Ni has an average configuration of $3d^{7.33}$, which is a configuration more readily achieved by Co.

Can the research approach of this work be applied to cuprates? That is, can a cuprate high-temperature superconductor similar to $\text{La}_3\text{Ni}_2\text{O}_7$ be realized? Previous studies [28, 29] have indicated that cuprates cannot realize two-orbital strong correlations, nor can they achieve two-orbital high-temperature superconductivity akin to that in $\text{La}_3\text{Ni}_2\text{O}_7$.

Iron-based materials are known to exhibit five-orbital high-temperature superconductivity. Furthermore, Co is adjacent to Fe in the periodic table. Therefore, designing Co-based superconductors analogous to iron-based ones presents another potential route to realizing cobalt-based high-temperature superconductivity.

This work was supported by the National Key R&D Program of China (Grants No. 2024YFA1408601 and No. 2024YFA1408602) and the National Natural Science Foundation of China (Grant No. 12434009). J.X.W. was also supported by the Outstanding Innovative Talents Cultivation Funded Programs 2025 of Renmin University of China. Z.Y.L. was also supported by the In-

novation Program for Quantum Science and Technology (Grant No. 2021ZD0302402). Computational resources were provided by the Physical Laboratory of High Performance Computing in Renmin University of China.

* These authors contributed equally to this work.

† rqhe@ruc.edu.cn

‡ zlu@ruc.edu.cn

- [1] C. W. Chu, P. H. Hor, R. L. Meng, L. Gao, and Z. J. Huang, Superconductivity at 52.5 K in the lanthanum-barium-copper-oxide system, *Science* **235**, 567 (1987).
- [2] A. Schilling, M. Cantoni, J. Guo, and H. Ott, Superconductivity above 130 K in the Hg – Ba – Ca – Cu – O system, *Nature* **363**, 56 (1993).
- [3] S. Putlin, E. Antipov, O. Chmaissem, and M. Marezio, Superconductivity at 94 K in $\text{HgBa}_2\text{CuO}_{4+\delta}$, *Nature* **362**, 226 (1993).
- [4] C. Park and R. L. Snyder, Structures of high-temperature cuprate superconductors, *Journal of the American Ceramic Society* **78**, 3171 (1995).
- [5] Y. Kamihara, T. Watanabe, M. Hirano, and H. Hosono, Iron-based layered superconductor $\text{La}[\text{O}_{1-x}\text{F}_x]\text{FeAs}$ ($x = 0.05\text{--}0.12$) with $T_c = 26$ K, *Journal of the American Chemical Society* **130**, 3296 (2008).
- [6] M. Rotter, M. Tegel, and D. Johrendt, Superconductivity at 38 K in the iron arsenide $(\text{Ba}_{1-x}\text{K}_x)\text{Fe}_2\text{As}_2$, *Phys. Rev. Lett.* **101**, 107006 (2008).
- [7] D. C. Johnston, The puzzle of high temperature superconductivity in layered iron pnictides and chalcogenides, *Advances in Physics* **59**, 803 (2010).
- [8] D. Li, B. Y. Wang, K. Lee, S. P. Harvey, M. Osada, B. H. Goodge, L. F. Kourkoutis, and H. Y. Hwang, Superconducting dome in $\text{Nd}_{1-x}\text{Sr}_x\text{NiO}_2$ infinite layer films, *Physical Review Letters* **125**, 027001 (2020).
- [9] D. Li, K. Lee, B. Y. Wang, M. Osada, S. Crossley, H. R. Lee, Y. Cui, Y. Hikita, and H. Y. Hwang, Superconductivity in an infinite-layer nickelate, *Nature* **572**, 624 (2019).
- [10] H. Sun, M. Huo, X. Hu, J. Li, Z. Liu, Y. Han, L. Tang, Z. Mao, P. Yang, B. Wang, *et al.*, Signatures of superconductivity near 80 K in a nickelate under high pressure, *Nature* **621**, 493 (2023).
- [11] Y. Zhu, D. Peng, E. Zhang, B. Pan, X. Chen, L. Chen, H. Ren, F. Liu, Y. Hao, N. Li, *et al.*, Superconductivity in pressurized trilayer $\text{La}_4\text{Ni}_3\text{O}_{10-\delta}$ single crystals, *Nature* **631**, 531 (2024).
- [12] A. S. Botana and M. R. Norman, Similarities and differences between LaNiO_2 and CaCuO_2 and implications for superconductivity, *Phys. Rev. X* **10**, 011024 (2020).
- [13] V. V. Poltavets, M. Greenblatt, G. H. Fecher, and C. Felser, Electronic properties, band structure, and fermi surface instabilities of $\text{Ni}^{1+}/\text{Ni}^{2+}$ nickelate $\text{La}_3\text{Ni}_2\text{O}_6$, isoelectronic with superconducting cuprates, *Phys. Rev. Lett.* **102**, 046405 (2009).
- [14] V. V. Poltavets, K. A. Lokshin, A. H. Nevidomskyy, M. Croft, T. A. Tyson, J. Hadermann, G. Van Tendeloo, T. Egami, G. Kotliar, N. ApRoberts-Warren, A. P. Dioguardi, N. J. Curro, and M. Greenblatt, Bulk magnetic order in a two-dimensional $\text{Ni}^{1+}/\text{Ni}^{2+}$ (d^9/d^8) nickelate, isoelectronic with superconducting cuprates, *Phys. Rev.*

- Lett.* **104**, 206403 (2010).
- [15] H. Sakakibara, H. Usui, K. Suzuki, T. Kotani, H. Aoki, and K. Kuroki, Model construction and a possibility of cupratelike pairing in a new d^9 nickelate superconductor (Nd,Sr)NiO₂, *Phys. Rev. Lett.* **125**, 077003 (2020).
 - [16] K. Takada, H. Sakurai, E. Takayama-Muromachi, F. Izumi, R. A. Dilanian, and T. Sasaki, Superconductivity in two-dimensional CoO₂ layers, *Nature* **422**, 53 (2003).
 - [17] I. Mazin and M. Johannes, A critical assessment of the superconducting pairing symmetry in $\text{Na}_x\text{CoO}_2 \cdot y\text{H}_2\text{O}$, *Nature Physics* **1**, 91 (2005).
 - [18] J. W. Lynn, Q. Huang, C. M. Brown, V. L. Miller, M. L. Foo, R. E. Schaak, C. Y. Jones, E. A. Mackey, and R. J. Cava, Structure and dynamics of superconducting Na_xCoO_2 hydrate and its unhydrated analog, *Phys. Rev. B* **68**, 214516 (2003).
 - [19] J. Cheng, J. Bai, B. Ruan, P. Liu, Y. Huang, Q. Dong, Y. Huang, Y. Sun, C. Li, L. Zhang, Q. Liu, W. Zhu, Z. Ren, and G. Chen, Superconductivity in a layered cobalt oxychalcogenide $\text{Na}_2\text{CoSe}_2\text{O}$ with a triangular lattice, *Journal of the American Chemical Society* **146**, 5908 (2024).
 - [20] Z. Wu, Y. Cao, H.-G. Luo, and Y.-f. Yang, Weak electronic correlations in the cobalt oxychalcogenide superconductor $\text{Na}_2\text{CoSe}_2\text{O}$, *arXiv preprint arXiv:2501.09675* (2025).
 - [21] S. Graser, T. A. Maier, P. J. Hirschfeld, and D. J. Scalapino, Near-degeneracy of several pairing channels in multiorbital models for the Fe pnictides, *New J. Phys.* **11**, 025016.
 - [22] A. F. Kemper, T. A. Maier, S. Graser, H.-P. Cheng, P. J. Hirschfeld, and D. J. Scalapino, Sensitivity of the superconducting state and magnetic susceptibility to key aspects of electronic structure in ferropnictides, *New J. Phys.* **12**, 073030.
 - [23] Y. Huan, S. Chen, R. Zeng, T. Wei, D. Dong, X. Hu, and Y. Huang, Intrinsic effects of ruddlesden-popper-based bifunctional catalysts for high-temperature oxygen reduction and evolution, *Advanced Energy Materials* **9**, 1901573 (2019).
 - [24] Z. Luo, X. Hu, M. Wang, W. Wú, and D.-X. Yao, Bilayer two-orbital model of $\text{La}_3\text{Ni}_2\text{O}_7$ under pressure, *Phys. Rev. Lett.* **131**, 126001 (2023).
 - [25] Z. Ouyang, J.-M. Wang, J.-X. Wang, R.-Q. He, L. Huang, and Z.-Y. Lu, Hund electronic correlation in $\text{La}_3\text{Ni}_2\text{O}_7$ under high pressure, *Phys. Rev. B* **109**, 115114 (2024).
 - [26] Z. Ouyang, R.-Q. He, and Z.-Y. Lu, Phase diagrams and two key factors to superconductivity of ruddlesden-popper nickelates, *Phys. Rev. B* **112**, 045127 (2025).
 - [27] Y. Gao, W. Wu, Z. Liu, K. Held, and L. Si, Topotactical hydrogen induced single-band d -wave superconductivity in La_2NiO_4 , *Phys. Rev. Lett.* **135**, 026002 (2025).
 - [28] J.-H. She, J.-X. Wang, R.-Q. He, and Z.-Y. Lu, Absence of two-orbital superconductivity in cuprate family: A DFT+DMFT perspective (2025), *arXiv:2509.08823 [cond-mat.supr-con]*.
 - [29] J.-X. Wang, R.-Q. He, and Z.-Y. Lu, Correlated electronic structure of high-temperature superconductor $\text{Ba}_2\text{CuO}_{3+\delta}$ (2025), *arXiv:2507.11454 [cond-mat.supr-con]*.